Electronic Supplementary Material (ESI) for Nanoscale Advances.
This journal is © The Royal Society of Chemistry 2020

Supporting Information

for

Stabilization of Reduced Copper on Ceria Aerogels for CO Oxidation

Catherine L. Pitman,[a] Ashley M. Pennington,[a] Todd H. Brintlinger,[b] Daniel E. Barlow,[c] Liam F. Esparraguera,[c] Rhonda M. Stroud,[b] Jeremy J. Pietron,[d] Paul A. DeSario,*[c] and Debra R. Rolison*[c]

[a]NRL/NRC Postdoctoral Associate, U.S. Naval Research Laboratory, Washington, D.C. 20375, United States

[b]Materials Science and Technology Division (Code 6300), U.S. Naval Research Laboratory, Washington, D.C. 20375, United States

[c]Chemistry Division (Code 6100), U.S. Naval Research Laboratory, Washington, D.C. 20375, United States

[d]Former Employee, Surface Chemistry Branch (Code 6170), U.S. Naval Research Laboratory, Washington, D.C. 20375, United States

Contents

I. Characterization 2
II. Catalysis 2

I. Characterization

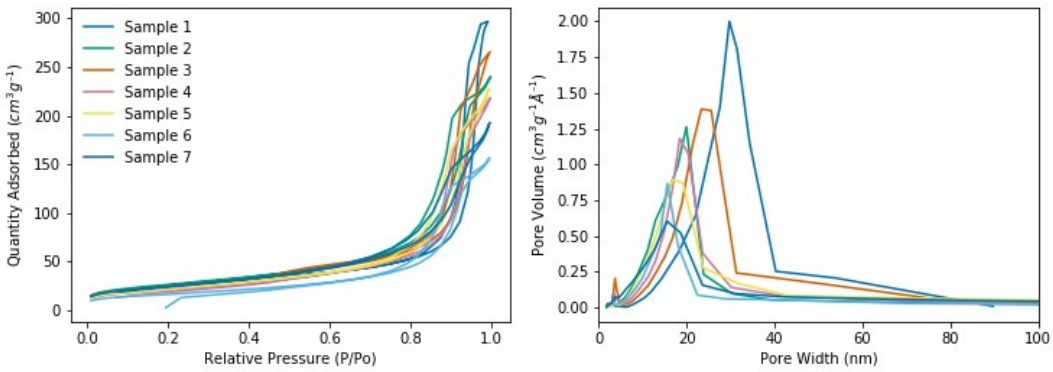

Fig. **S1** (left) N_2 adsorption and desorption isotherms of several different batches of CeO_2 aerogel. (right) BJH desorption pore width of several different batches of CeO_2 aerogel

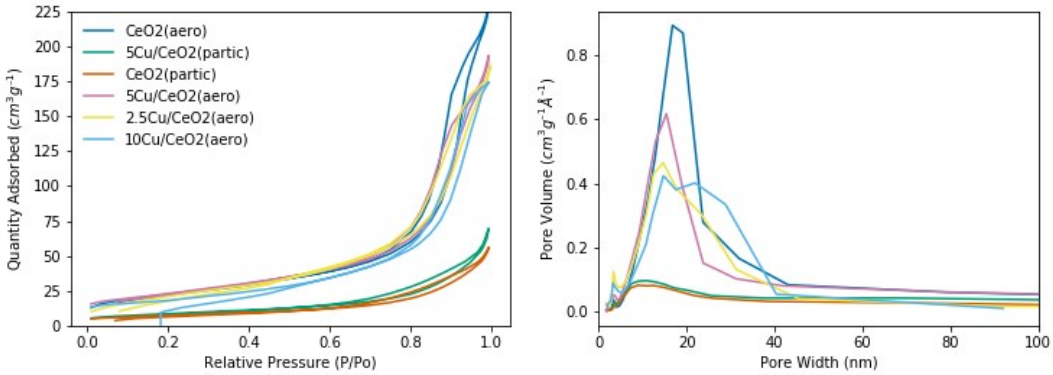

Fig. S2 (left) N_2 adsorption and desorption isotherms of CeO_2 and Cu/CeO_2 materials. (right) BJH desorption pore width of CeO_2 and Cu/CeO_2 materials.

Table S1. Porosimetry Data for Several Batches of CeO_2 aerogels

	BET SA (m^2/g)	BJH Ads Pore Volume (cm^3/g)	BJH Des Pore Volume (cm^3/g)	BJH Ads Pore Width 4V/A (nm)	BJH Des Pore Width 4V/A (nm)
Sample 1	85.0	0.46	0.46	22.5	21.0
Sample 2	95.0	0.37	0.37	15.8	14.6
Sample 3	89.0	0.41	0.41	18.2	16.6
Sample 4	76.8	0.34	0.34	17.1	15.1
Sample 5	81.5	0.35	0.35	17.0	15.7
Sample 6	59.2	0.24	0.23	15.9	13.1
Sample 7	89.3	0.29	0.30	12.8	12.3
Average	82.2	0.35	0.35	17.0	15.5
St Dev	11.7	0.07	0.08	2.9	2.8
High	95.0	0.46	0.46	22.5	21.0
Low	59.2	0.24	0.23	12.8	12.3

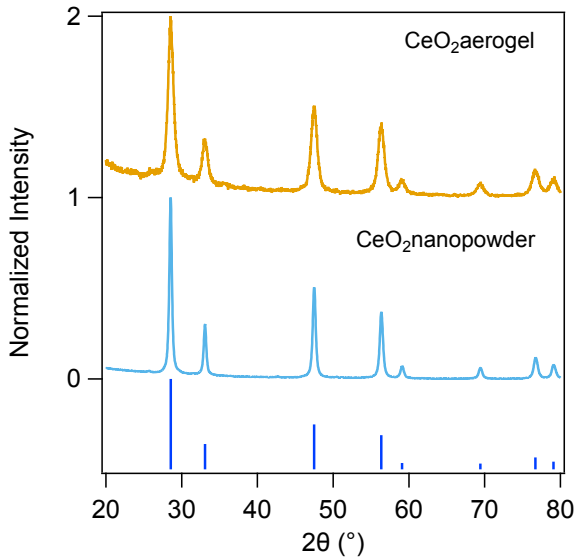

Fig. S3 Representative X-ray diffractometry of CeO_2(aero) and CeO_2(partic) materials compared to CeO_2 (JCPDS# 01-089-8436). Scherrer analysis of the CeO_2 (111) reflection at 2θ =28.55° with FWHM of 0.86(1)° and 0.38(1)° gives 9.4(9) nm and 21.3(6) nm particles for aerogel and particulate CeO_2, respectively.

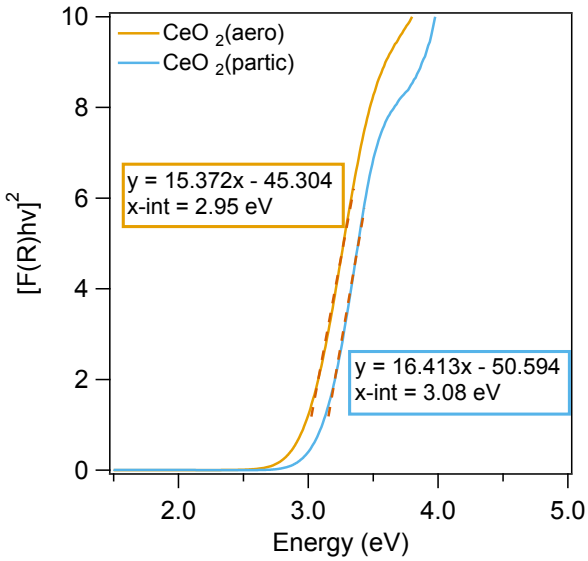

Fig. S4 Bandgap calculation for CeO_2(aero) (yellow) and CeO_2(partic) (blue) showing a smaller band gap for the aerogel sample (2.95 eV) vs the particulate sample (3.08 eV). Both of these band gaps are red-shifted from that of bulk CeO_2 (3.15 eV).

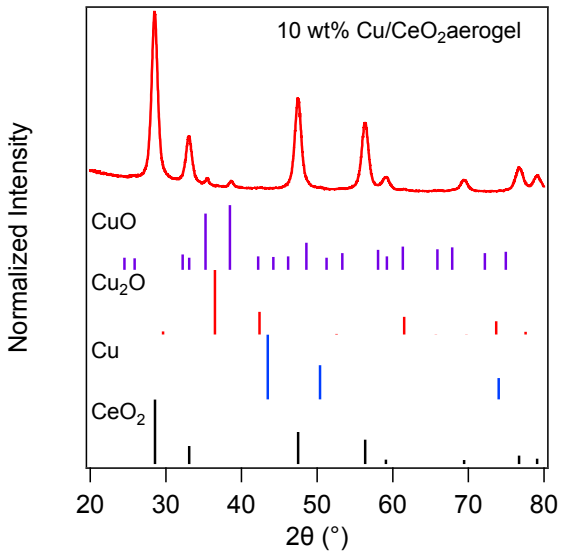

Fig. S5 X-ray diffractogram of a *10*Cu/CeO_2(aero) sample compared to the patterns for CuO (JCPDS# 00-044-0706), Cu_2O (JCPDS# 01-073-6237), Cu(JCPDS# 00-001-1241), and CeO_2 (JCPDS# 01-089-8436). Only reflections for CeO_2 and CuO could be identified.

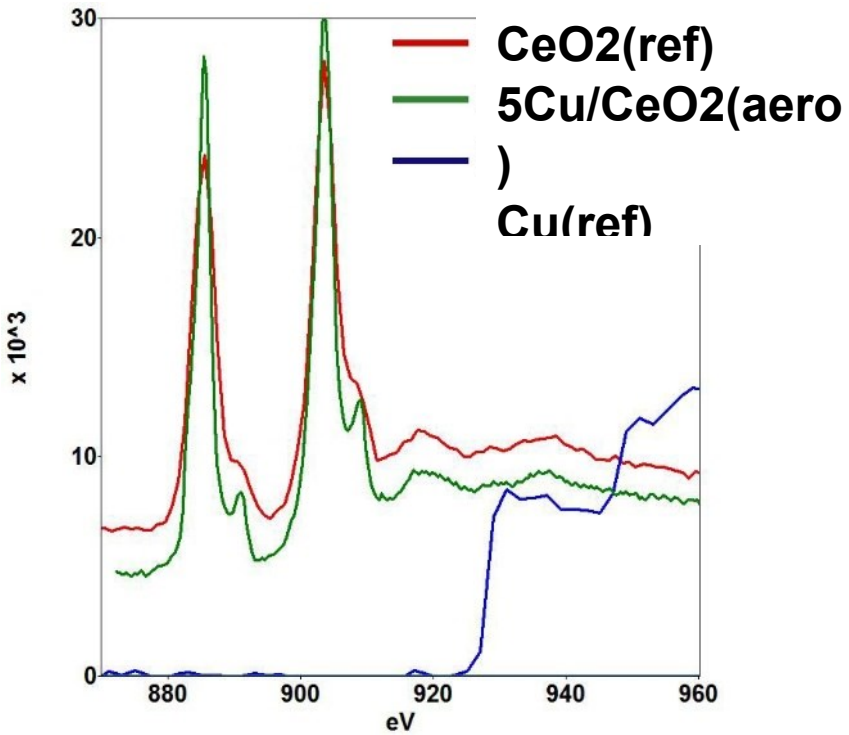

Figure S6. Electron energy–loss spectra illustrating peak overlap of Cu and CeO_2 core-loss as well as data acquired in this work; these spectra show how the various core-loss edges overlap between CeO_2 and Cu. While our data feature very little noise compared to reference data, the ability to distinguish copper L transitions on top of ceria M edges is extremely challenging, if not impossible.

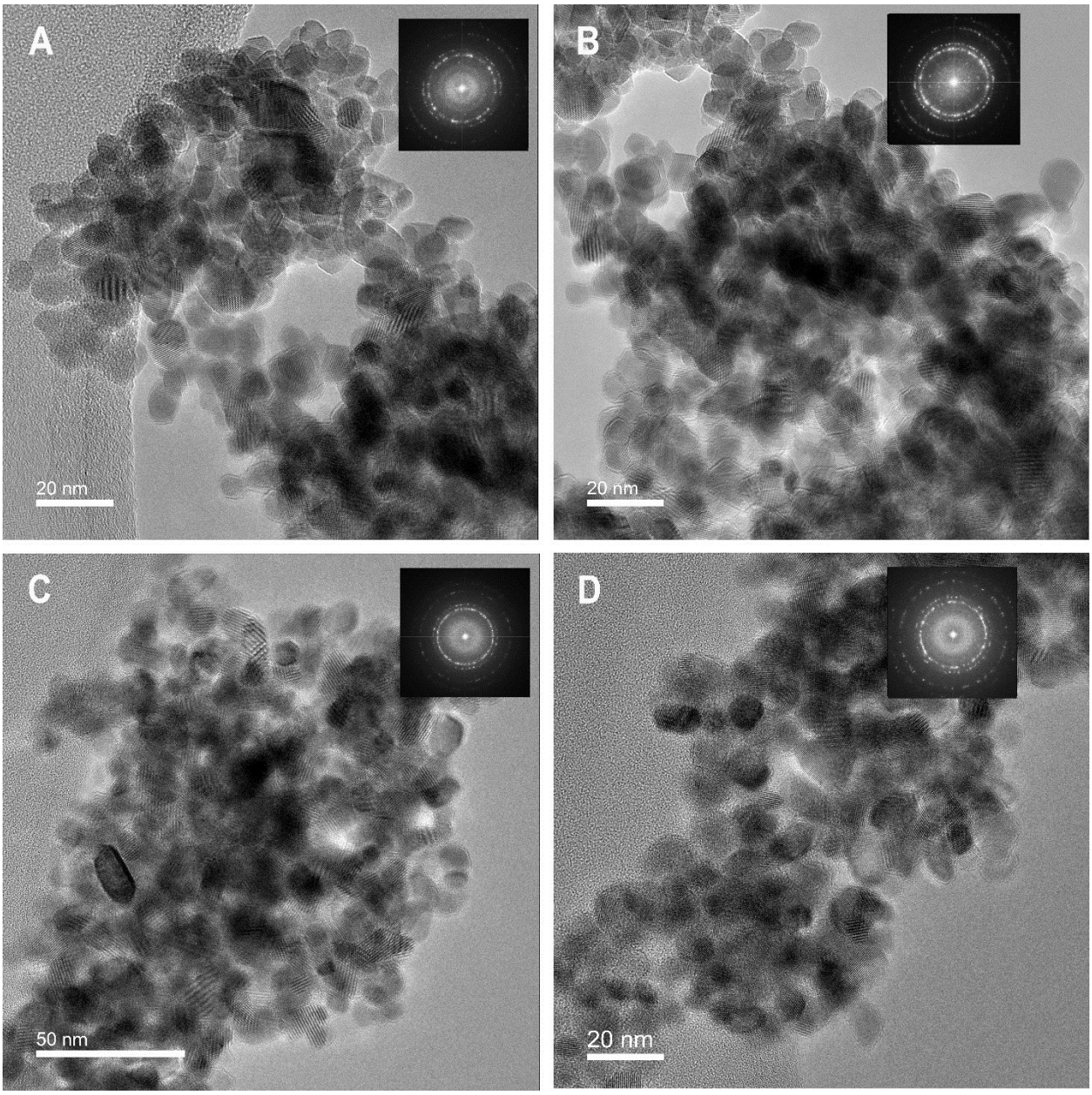

Fig. S7 High-resolution transmission electron micrographs of 5Cu/CeO_2(aero) structures. Panels A–D all show crystalline nanoparticles of ceria, as evidenced by lattice parameters corresponding to ceria <111> and <200> planes, seen in the FFT insets. Attempts to use FFT-filtering to circumvent difficulties associated with HAADF-intensity and/or spectroscopic identification (through energy-dispersive or electron energy–loss spectroscopy) did not prove successful as no lattice planes could be definitively identified as either Cu^0 or Cu^+. Ceria nanoparticles of the aerogel are readily identified, however, and consistently show similar morphology and crystallinity.

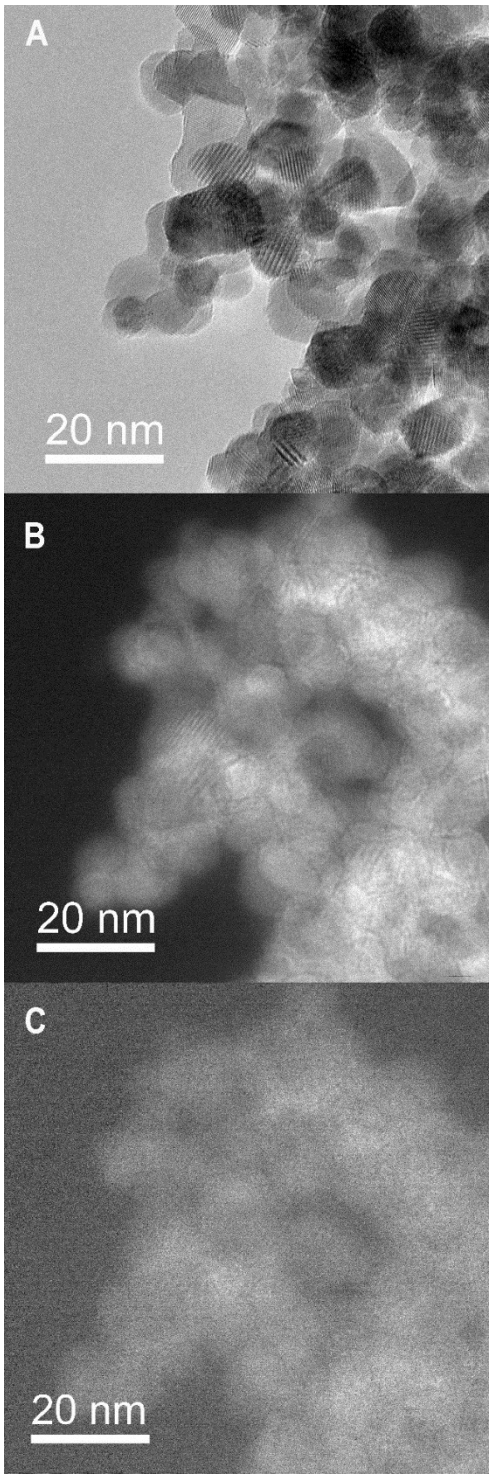

Fig. S8 Energy-filtered transmission electron microscopy (EF-TEM). (A) HR-TEM of small *5*Cu/CeO_2(aero) structure. (B) EF-TEM with slit at ~50 eV. (C) EF-TEM with slit at 100 eV. Both low-loss and high-loss energy-filtered transmission electron microscopy were performed, but significant amounts of peak overlap in both regions combined with the inherent difficulty of searching for lower-Z copper on higher-Z ceria together with a complex aerogel morphology make definitive identification of copper nanoparticles practically impossible.

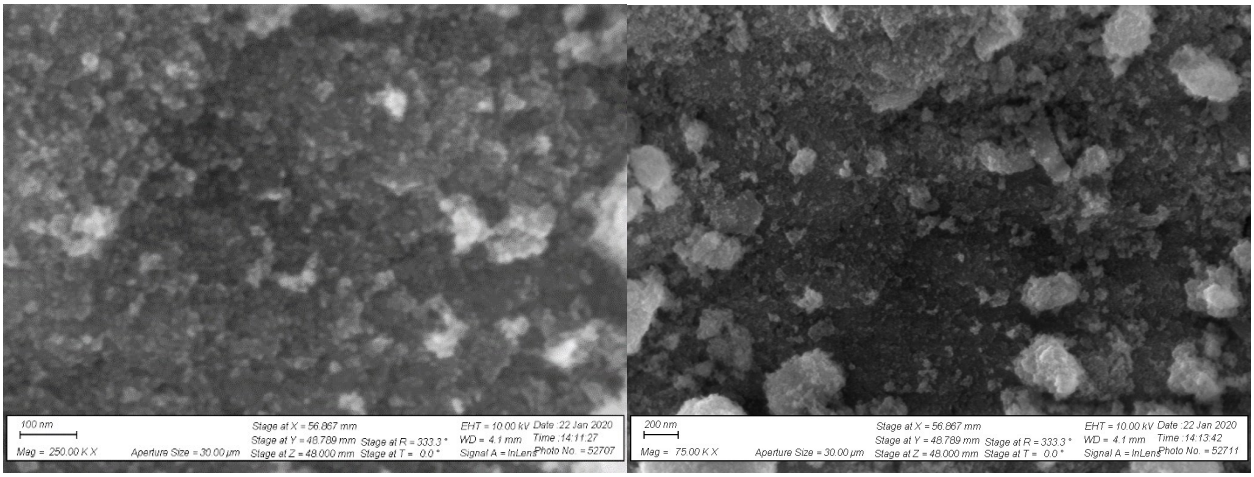

Fig. S9 Scanning electron micrographs of *5*Cu/CeO_2(aero) at (left) 250 KX and (right) 75 KX magnification.

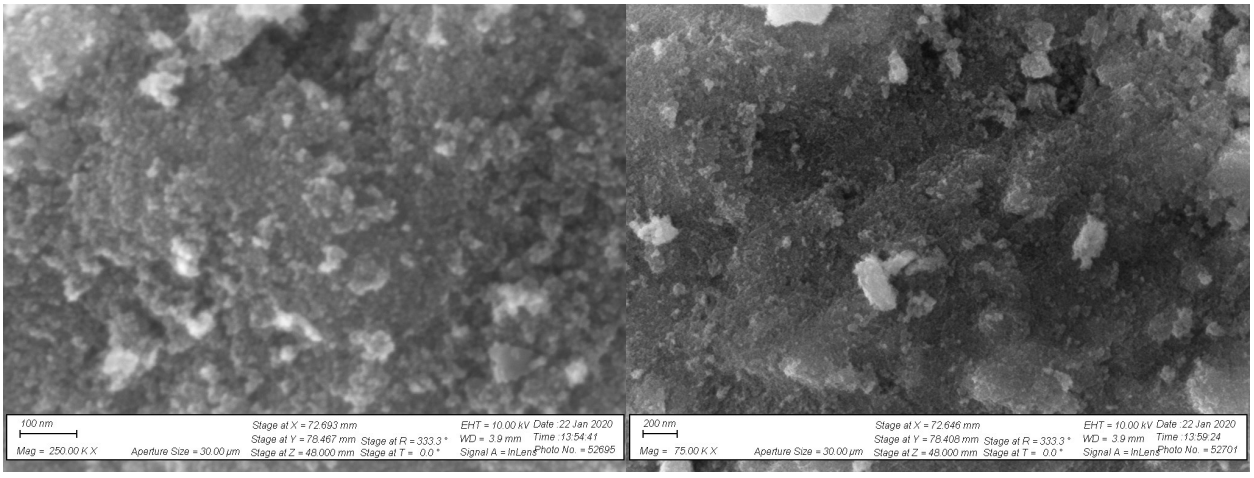

Fig. S10 Scanning electron micrographs of *2.5*Cu/CeO_2(aero) at (left) 250 KX and (right) 75 KX magnification.

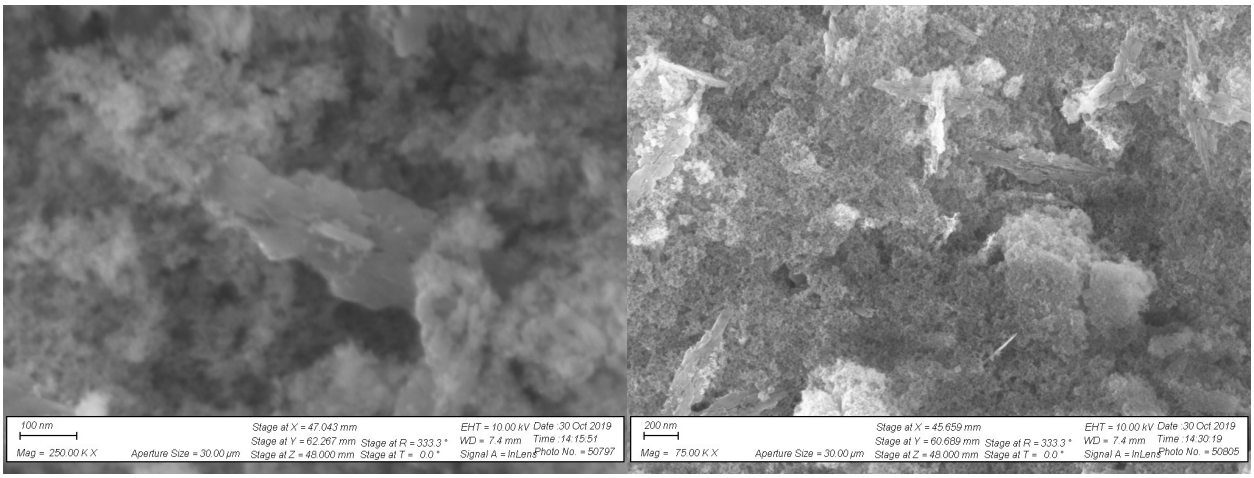

Fig. S11 Scanning electron micrographs of *10*Cu/CeO_2(aero) at (left) 250 KX and (right) 75 KX magnification showing the platelet structures formed after Cu photodeposition and their prevalence on the surface.

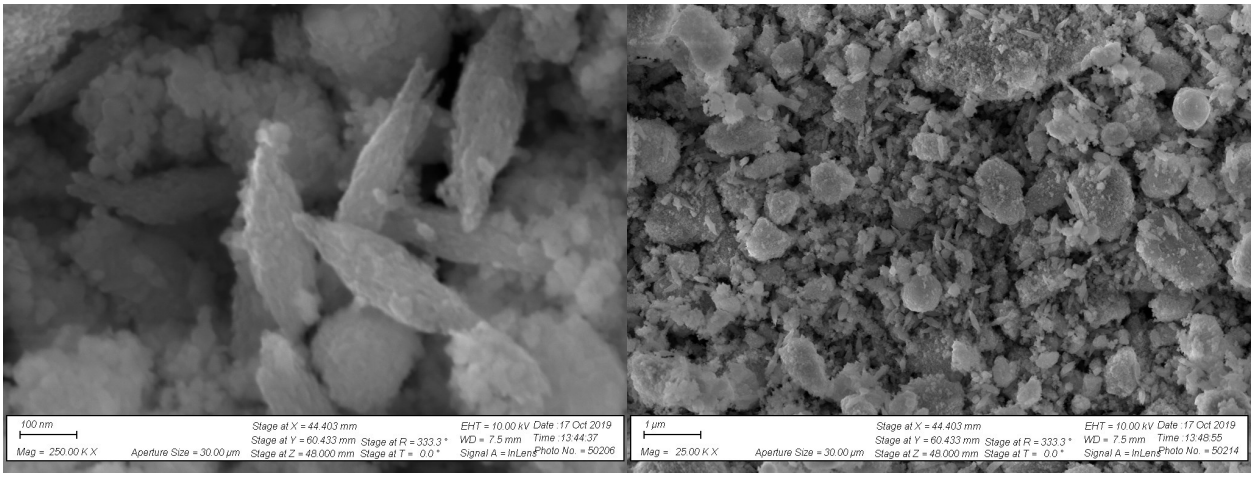

Fig. S12 Scanning electron micrographs of *5*Cu/CeO_2(partic) at (left) 250 KX and (right) 75 KX magnification showing the bicone structures formed after Cu photodeposition and their prevalence on the surface.

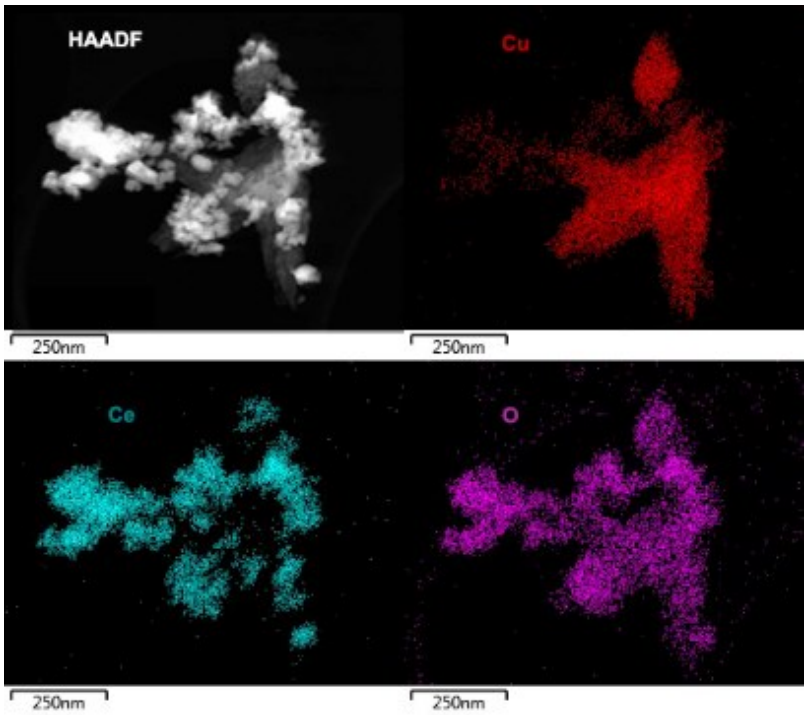

Fig. S13 Energy-dispersive spectroscopy mapping of *5*Cu/CeO_2(partic) showing the localization of Cu in the large bicone features.

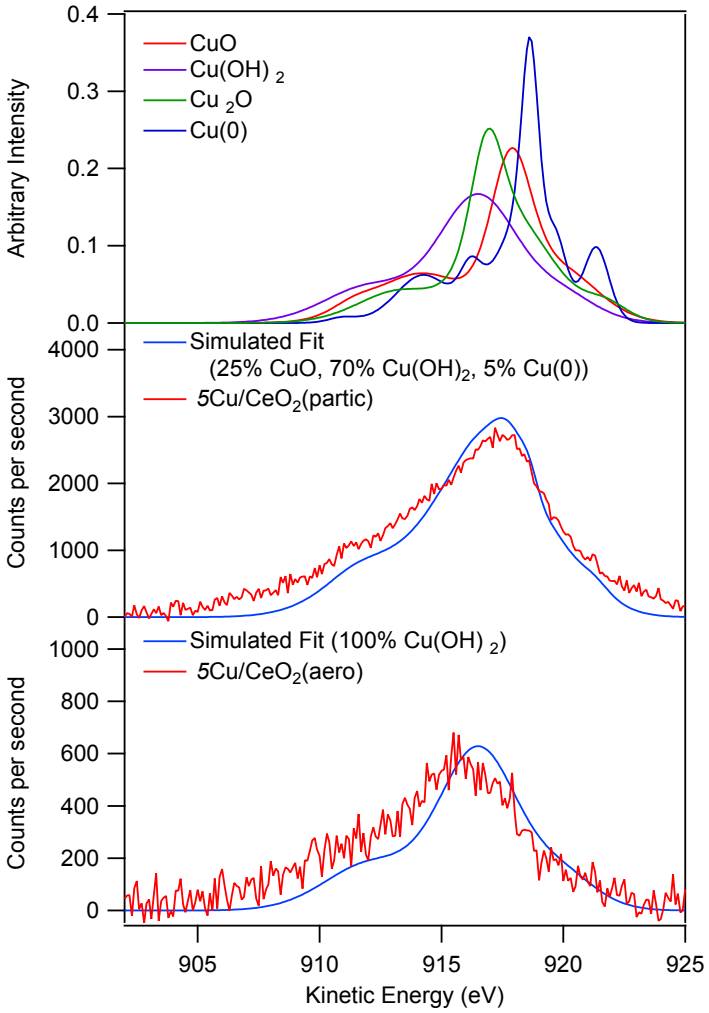

Fig. S14 (top) Cu LMM of the four most likely Cu states with the peak shapes determined from Biesinger.[1] (middle) *5*Cu/CeO_2(partic) Cu LMM and best fit of the data using fitting components. (bottom) *5*Cu/CeO_2(aero) Cu LMM and best fit of the data using fitting components. Due to the mixture of oxidation states, peak broadening of insulating materials, and low Cu content, satisfactory fits for quantification of oxidation states could not be obtained.

II. Catalysis

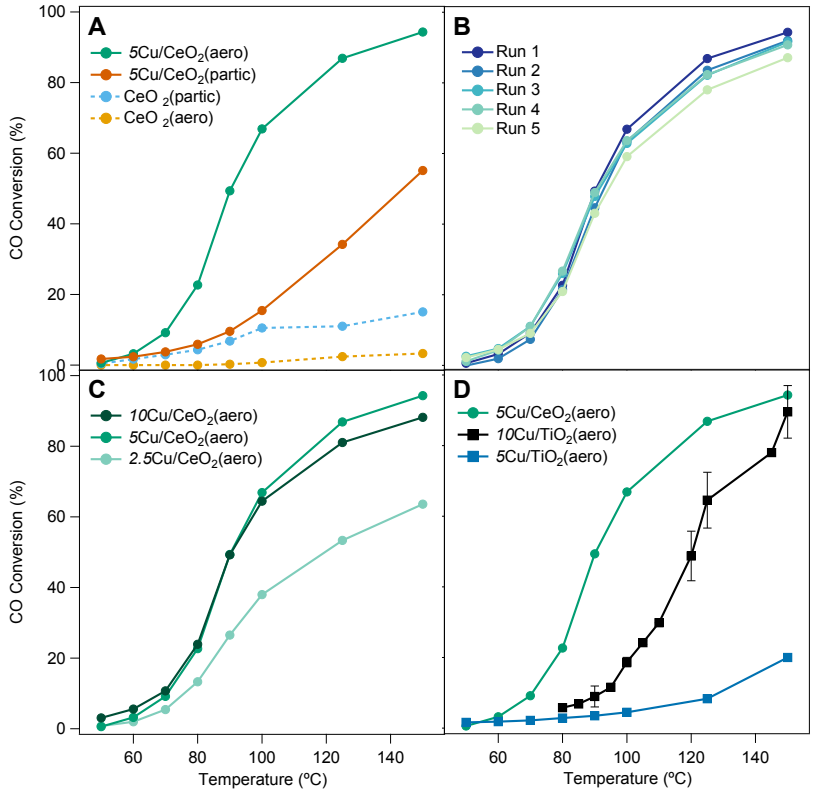

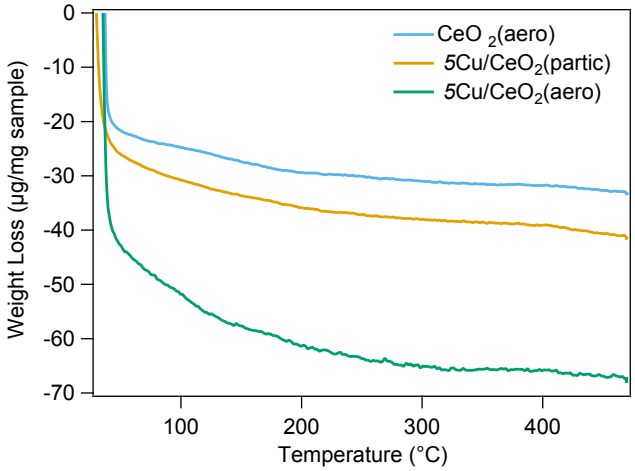

Fig. S16 Thermogravimetric analysis of different catalytic samples. If the entire mass loss is assigned to carbon (which is an overestimate neglecting water loss and any H/O bound to C), the highest weight loss we observed (0.068 mg loss/mg sample) accounts for just under 2 min of CO_2 production (if we assume

Fig. S15 CO conversion as a percentage versus temperature for (A) catalysts with different CeO_2 supports: 5Cu/CeO_2(aero) (green), 5Cu/CeO_2(partic) (amber), CeO_2(aero) (dashed yellow), and CeO_2(partic) (dashed blue); (B) 5 runs of 5Cu/CeO_2(aero) separated by regeneration of the catalyst bed; (C) different weight loadings of Cu on CeO_2(aero): 10Cu/CeO_2(aero) (dark green), 5Cu/CeO_2(aero) (green), and 2.5Cu/CeO_2(aero) (light green); and (D) catalysts with CeO_2 vs TiO_2 supports: 5Cu/CeO_2(aero) (green), 5Cu/TiO_2(aero) (blue), and 10Cu/TiO_2(aero) (black)

100% "CO Conversion"). This amount is dramatically less than the amount of CO consumed, so it is likely not a major component of catalysis.

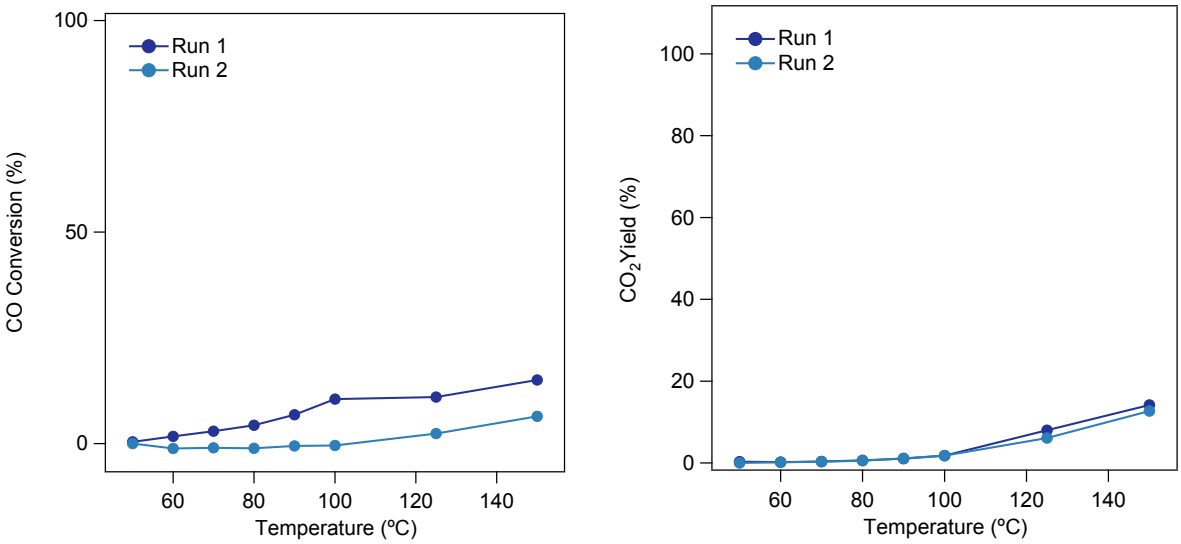

Fig. S17 CO conversion (left) and CO_2 yield (as a percentage of total CO introduced) for two catalytic runs of CeO_2(partic).

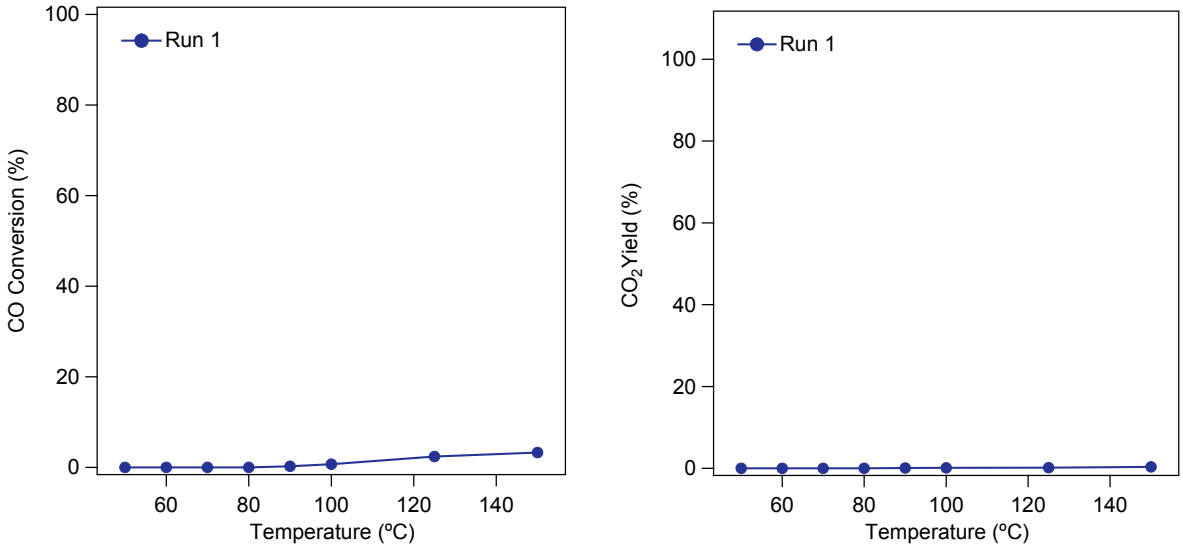

Fig. S18 CO conversion (left) and CO_2 yield (as a percentage of total CO introduced) for one catalytic run of CeO_2(aero).

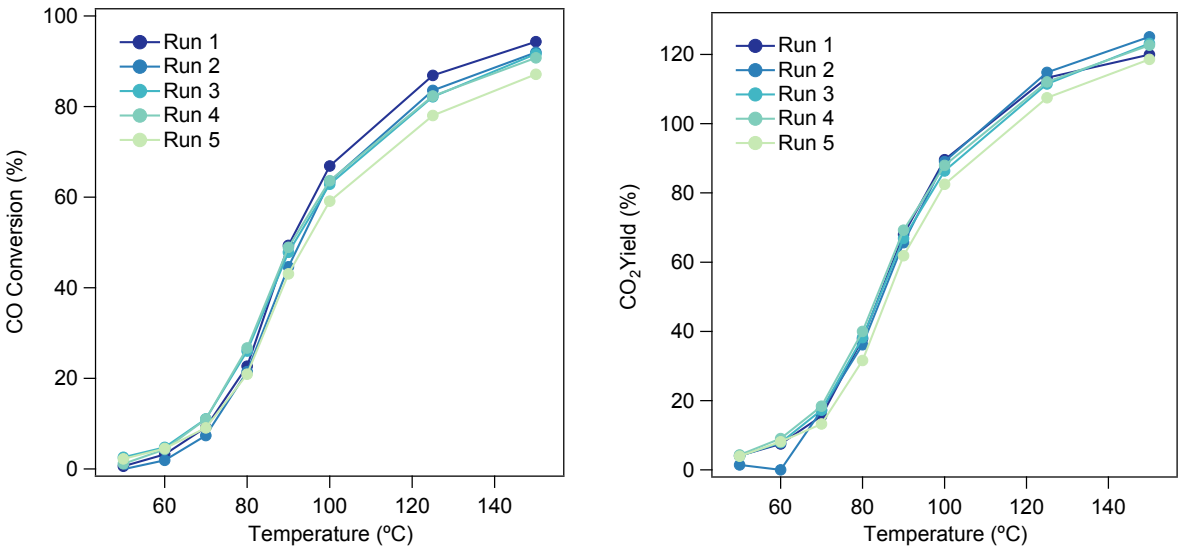

Fig. S19 CO conversion (left) and CO_2 yield (as a percentage of total CO introduced) for 5 catalytic runs of *5*Cu/CeO_2(aero).

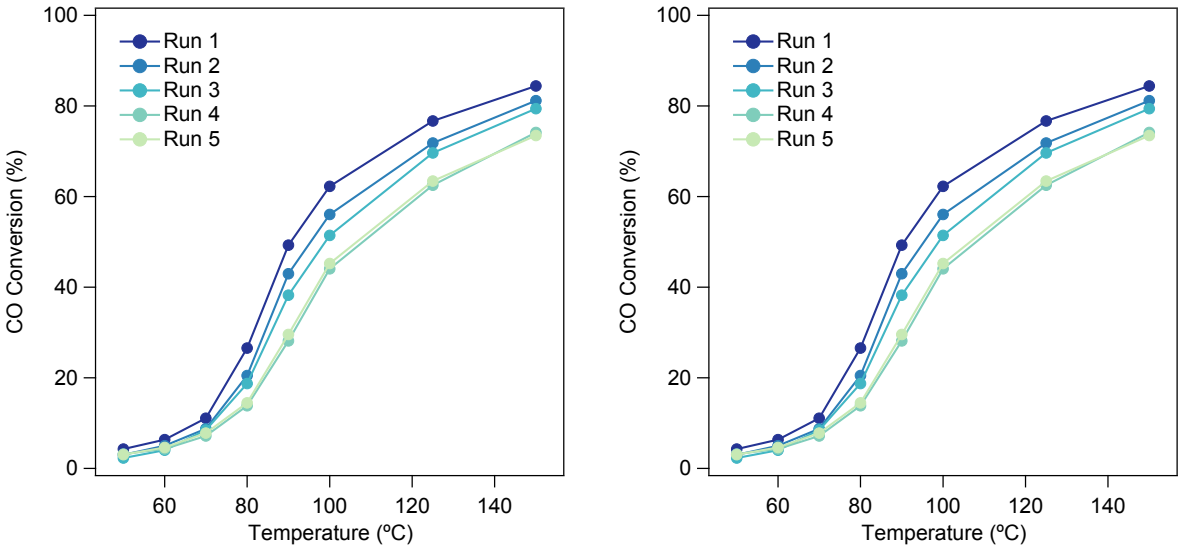

Fig. S20 CO conversion (left) and CO_2 yield (as a percentage of total CO introduced) for 5 catalytic runs of separate batch of *5*Cu/CeO_2(aero).

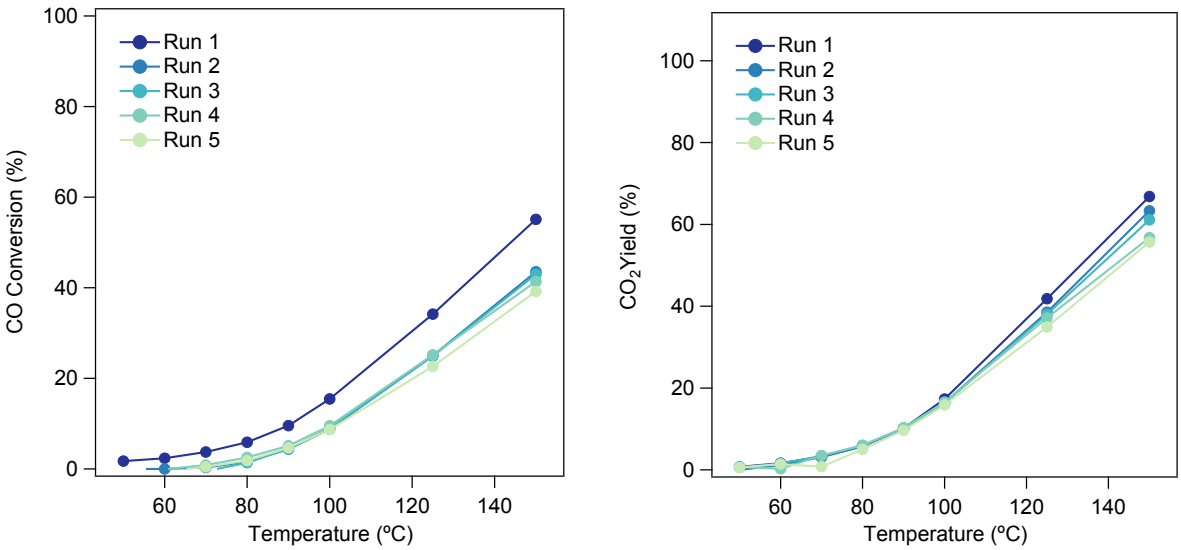

Fig. S21 CO conversion (left) and CO_2 yield (as a percentage of total CO introduced) for 5 catalytic runs of *5*Cu/CeO_2partic).

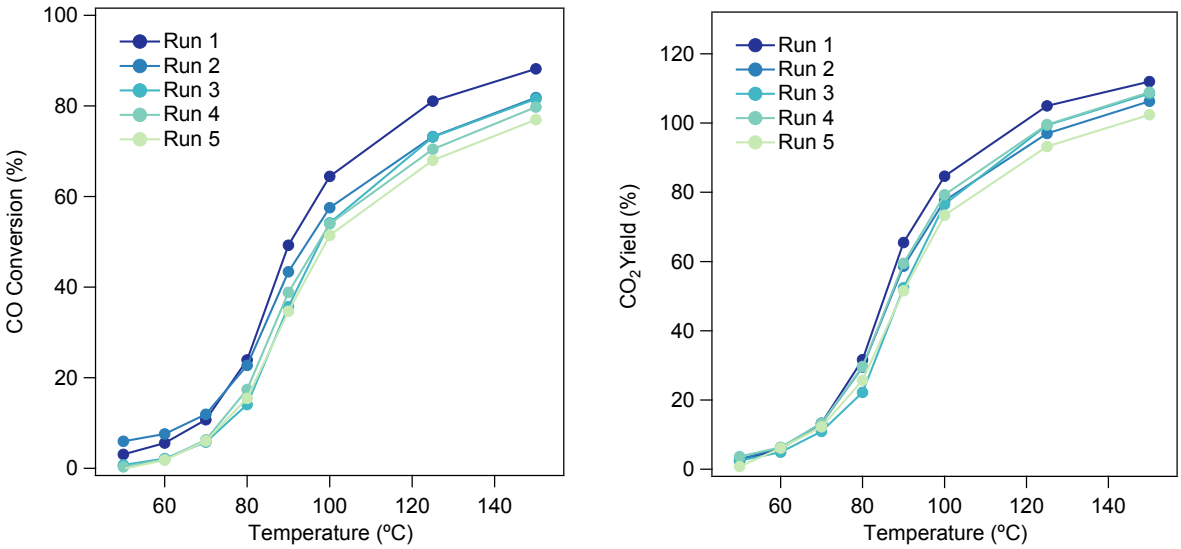

Fig. S22 CO conversion (left) and CO_2 yield (as a percentage of total CO introduced) for 5 catalytic runs of *10*Cu/CeO_2(aero).

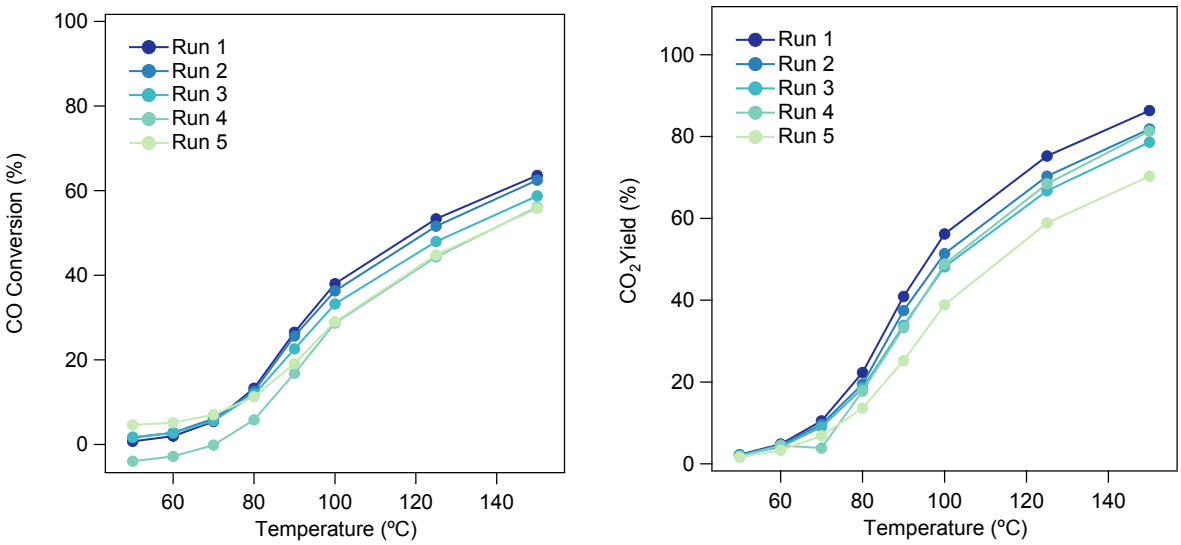

Fig. S23 CO conversion (left) and CO_2 yield (as a percentage of total CO introduced) for 5 catalytic runs of 2.5Cu/CeO_2(aero).

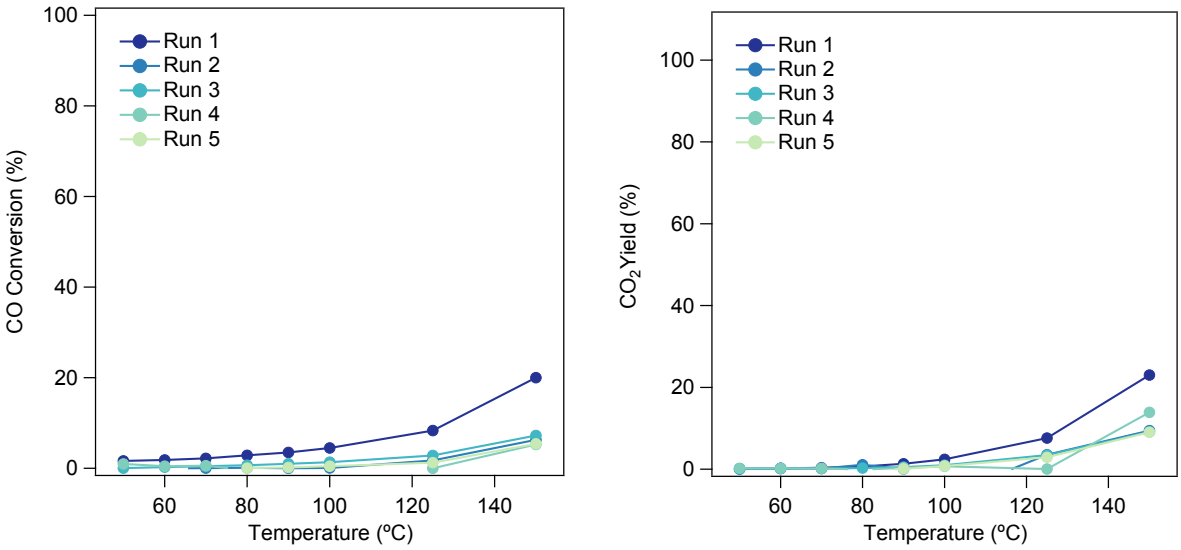

Fig. S24 CO conversion (left) and CO_2 yield (as a percentage of total CO introduced) for 5 catalytic runs of *5*Cu/TiO_2(aero).

Table S2. Sensitivity Analysis of Activation Energy Calculation from CO Conversion (kJ/mol)

	3% Higher	1.5% Higher	As calculated	1.5% Lower	3% Lower
*5*Cu/CeO_2(partic)	38.8	48.8	66.8	114.7	167.4
*2.5*Cu/CeO_2(aero)	63.8	74.3	90.1	119.7	164.1
*5*Cu/CeO_2(aero)	54.0	64.1	79.4	106.2	179.0
*10*Cu/CeO_2(aero)	68.9	78.1	90.5	108.8	140.0

*10*Cu/CeO_2(aero)	48.1	72.9	83.5	130.9	167.2
*5*Cu/TiO_2(aero)	59.7	65.7	73.4	83.6	98.2

Under these flow conditions, the CO stream varies by 3%. To assess the impact of a 3% variation of the CO stream on the low-conversion conditions required for calculating activation energies, a sensitivity analysis was performed. We find that a 3% variation produces such a large range of activation energy values for the calculated values to be essentially meaningless.

[1] M. C. Biesinger *Surf. Interface Anal*. 2017, **49**, 1325–1334 (10.1002/sia.6239)